Available online at www.sciencedirect.com
ScienceDirect
Dyes and Pigments 77 (2008) 515–524
DYES and PIGMENTS
www.elsevier.com/locate/dyepig

Nonlinear optical polyimide/montmorillonite nanocomposites consisting of azobenzene dyes

Tsung-Yi Chao [a], Huey-Ling Chang [b,**], Wen-Chiung Su [c], Jeng-Yue Wu [a], Ru-Jong Jeng [a,*]

[a] Department of Chemical Engineering, National Chung Hsing University, 250 Kuo-Kuang Road, Taichung 402, Taiwan
[b] Department of Chemical and Materials Engineering, National Chinyi University of Technology, Taichung 411, Taiwan
[c] Chung Shan Institute of Science and Technology, Lungtan, Taoyuan 325, Taiwan

Received 29 May 2007; received in revised form 1 August 2007; accepted 2 August 2007
Available online 19 August 2007

Abstract

A reactive organoclay was formed using trifunctional 1,1,1-tris[4-(4-amino-2-trifluoromethylphenoxy)phenyl] as a swelling agent for the silicate layers of montmorillonite. One of the functional groups of the swelling agents formed an ionic bond with the negatively charged silicates, whereas the remaining functional groups were available for further reaction with poly(amic acid) end capped with anhydride groups. Subsequently, the hydroxyl groups of the ensuing polyimide could be further reacted with isocyanate-containing dyes to form nonlinear optical polyimides with high T_gs. X-ray diffraction and transmission electron microscopy revealed that the dispersion of silicate layers in the polyimide created an exfoliated structure as a result of using the trifunctional groups of the swelling agent. This particular structure of the nanocomposite resulted in enhanced thermal properties and excellent optical transparency. Using in situ contact poling, r_{33} coefficients ranging from 4.6 to 7.6 pm/V were obtained for the organic/inorganic NLO materials; excellent temporal stability at 100 °C was obtained.

Keywords: Dye; Exfoliate; Montmorillonite (MMT); NLO; Polyimide; EO coefficient

1. Introduction

Second-order nonlinear optical (NLO) polymers have been extensively studied for applications in optical communication, optical data storage, optical switching and frequency modulation because of their large optical nonlinearity, fast response, and easy processing for integrated assembly [1,2]. Large optical nonlinearity, excellent temporal stability of dipole orientation, and low optical loss are important challenges to material scientists in designing second-order NLO materials [3,4].

The major drawback of NLO polymers is the decay of electric field induced second-order optical nonlinearity. There are many efficient ways to prevent the randomization of the poled order, including incorporating high glass transition temperature (T_g), crosslinking, and/or IPN features [5–8]. Among various polymers, aromatic polyimides have been selected as one of the promising candidates to overcome the above-mentioned problem. This is because their high T_g feature would warrant excellent NLO stability at elevated temperatures [9–11]. Several approaches have been reported to enhance the stability and processability of NLO material based on polyimides [12]. Jeng et al. have reported a second-order NLO organic/inorganic composite based on an alkoxysilane dye (ASD) and an aromatic polyimide [13]. Organically modified inorganic NLO sol–gel materials are obtained via incorporation of the organic NLO-active dye into an alkoxysilane-based inorganic network. Moreover, the formation of three-dimensional silicon oxide networks via in situ sol–gel process would prevent the randomization of poled NLO dye in the absence of a poling field. As a result, long-termed NLO stability at elevated temperatures was greatly enhanced. However, this enhancement usually requires the presence of

* Corresponding author. Tel.: +886 4 22852581; fax: +886 4 22854734.
** Corresponding author.
E-mail address: rjjeng@nchu.edu.tw (R.-J. Jeng).

0143-7208/$ - see front matter © 2007 Elsevier Ltd. All rights reserved.
doi:10.1016/j.dyepig.2007.08.001

large quantities of the inorganic sol–gel materials in polymer matrices [13]. This would lead to the reduction of dye content, which means the decrease of optical nonlinearity.

Polymer/montmorillonite (MMT) nanocomposites have gained considerable interest in recent years owing to substantial improvements over their pristine states in thermal, mechanical, and gas barrier properties by incorporating only few (by weight percent) layered silicates, dispersed in the nanometer scale [14–17]. MMT consists of anionically charged layers of magnesium/aluminum silicates and small cations such as sodium or potassium located in silicate interlayer galleries [18]. In addition, MMT is hydrophilic because of the presence of ionic bonds and the ability to form hydrogen bonds with water [19]. In order to be compatible with polymer molecules, MMT is usually modified with organics to become hydrophobic. Furthermore, the expanded interlayer spacings allow polymer molecules to enter and subsequently to intercalate the silicate layers. As a result, depending on the sizes of the polymer molecules, the interlayer spacings of silicate can be formed with a distance of a few nanometers, or the silicate layers are exfoliated and dispersed in the polymer matrices.

Since the development of polyamide/MMT nanocomposite by Toyota's research group in 1990s [20,21], there have been a considerable number of publications describing the soluble polyimide/MMT nanocomposite materials [22–24]. Specifically, polyimide/MMT nanocomposites prepared from poly (amic acid) and MMT were reported [25,26]. Surfactants such as 12-aminododecanoic and dodecylamine were utilized as swelling agents for forming polyimide/clay nanocomposites. It is important to note that these swelling agents were basically nonreactive toward the poly(amic acid)s. The swelling agents remained in a form of low molecular weight compounds after imidization. This resulted in a negative impact on the thermal and mechanical properties. To solve this problem, Wei et al. utilized reactive swelling agents to prepare polyimide/MMT nanocomposites with enhanced thermal and mechanical properties [15,19]. Moreover, several researchers attempted to incorporate NLO dyes into the layered nanocomposites, but failed to acquire any optical nonlinearity [14,27]. In this research, a new strategy to design second-order nonlinear optical materials is presented. We report the investigation of NLO-active polyimide/MMT materials. A swelling agent with multi-functional groups was chosen. One of the functional groups would form an ionic bond with negatively charged silicates, whereas the rest of the two functional groups in the swelling agent are available for further reaction with poly(amic acid)s containing anhydride end groups. Moreover, post-functionalization has been employed to prepare NLO polymers in the past few years [28–30]. Through this means, the exposure of the NLO dyes to harsh polymerization conditions can be avoided. Therefore, the polyimide/clay materials would further react with an equal equivalent of reactive NLO dyes (DO3-ISO) to obtain a series of organic/inorganic NLO polymers. The resulting materials possess high T_g values, excellent thermal stability and good optical quality. The synthesis of the NLO-active polyimide/MMT nanocomposite is depicted in Scheme 1.

2. Experimental

2.1. Materials and instrumentation

All of the chemicals were purchased and used as received unless otherwise stated. The solvents were purified by distillation under reduced pressure over calcium hydride. Na^+-MMT, supplied by Nanocor Co., America, is a sodium type with a cationic exchange capacity (CEC) of 1.20 mequiv/g and surface area of 750 m^2/g.

Infrared spectra were recorded by using a Perkin Elmer Paragon 500 FT-IR Spectrophotometer. ^{1}H NMR spectra were obtained with a Varian Gemini-200 FT-NMR Spectrometer with chloroform-d and DMSO-d_6. Elemental analysis (EA) was performed on an F002 Heraeus CHN–O Rapid Elemental Analyzer employing acetanilide as a standard. DSC and TGA were performed under nitrogen atmosphere on a Seiko SII model SSC/5200. A heating rate of 10 °C/min was used for DSC and TGA. Thermal degradation temperature (T_d) is taken at 5% weight loss. X-ray powder diffraction (XRD) analysis was performed with Shimadzu SD-Dl using a Cu target at 35 kV, 30 mA. The d-spacing of MMT was analyzed by using Bragg's equation ($n\lambda = 2d \sin\theta$). The morphology of the polymer was also analyzed by Transmitting Electron Microscope (TEM; Zeiss EM 902A). TEM was operated at 80 kV and the samples of approximately 70 nm were microtomed at room temperature.

2.2. Synthesis of polyimide

Aromatic organosoluble polyimides were successfully synthesized by solution imidization techniques [10]. 2,2-Bis(3-amino-4-hydroxyphenyl)-hexafluoropropane (0.36626 g, 1 mmol) was dissolved in 5 ml of dried DMAc in a 50 ml flask. After the diamine was dissolved completely, 4,4′-oxydiphthalic anhydride (0.31021 g, 1 mmol) was added to the diamine solution in one portion. The mixture was stirred in an ice bath for 12 h and then heated at 160 °C for 2 h. The polyimide was separated and purified by several re-precipitations from THE solution into methanol, and then dried under vacuum. Yield: 86.3%. ^{1}H NMR (DMSO-d_6): $\delta = 7.20$–8.40 (m, Ar-H), 10.48 (s, –OH). IR (KBr): 1380 cm^{-1} (C–N), 1720 and 1780 cm^{-1} (C=O), 3340 cm^{-1} (OH).

2.3. Synthesis of isocyanate-containing dye, 4-((4′-nitrophenyl)azo)phenylisocyanate (DO3-ISO) (Scheme 2)

4-((4′-Nitrophenyl)azo)phenylisocyanate was synthesized by reacting Disperse Orange 3 (DO3) dye with triphosgene. DO3 (0.738 g, 3 mmol) was dissolved in 50 ml of dried toluene in a 250 ml flask and heated at 100 °C. After DO3 was dissolved completely, triphosgene (0.297 g, 1 mmol) was added to the DO3 solution in one portion. The mixture was heated at 100 °C for 5 h. DO3-ISO was separated and purified by filter and then dried under vacuum. Yield: 62.7%. $C_{13}H_8N_4O_3$ (268.1): Calcd C 58.21, H 3.01, N 20.89; Found C 58.02, H

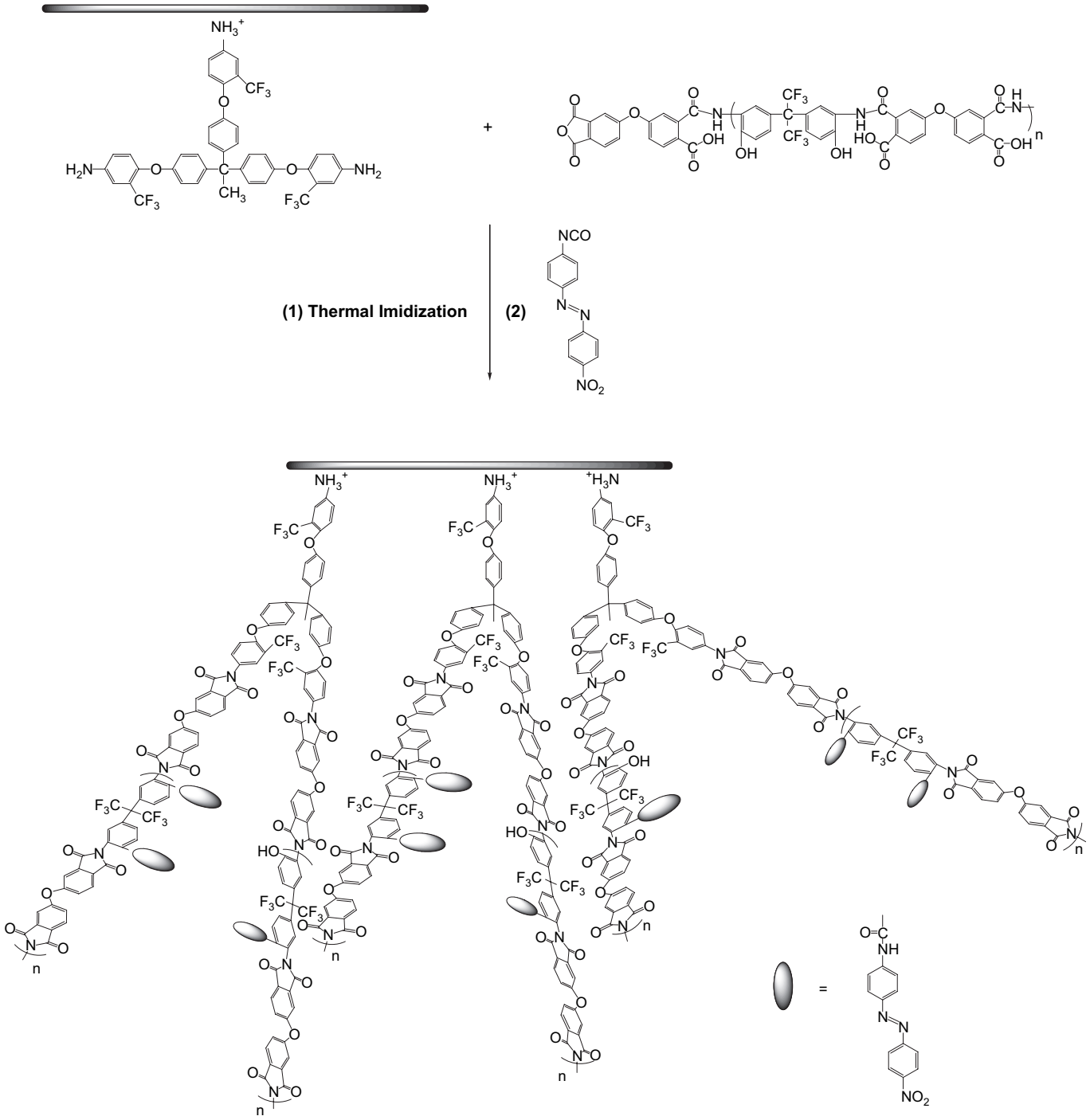

Scheme 1. Synthesis of NLO-active polyimide/MMT nanocomposite.

3.18, N 20.93. ^{1}H NMR ($CDCl_3$): $\delta = 7.20-8.40$ (m, Ar-H). IR (KBr): 2260 cm^{-1} (N═C═O), 1344 and 1525 cm^{-1} (NO_2).

*2.4. Synthesis of 1,1,1-tris[4-(4-nitro-2-trifluoromethylphenoxy)phenyl]ethane (compound **1**) (Scheme 3)*

1,1,1-Tris-(hydroxyphenyl)ethane (THPE) (0.613 g, 2 mmol) and 2-chloro-5-nitrobenzotrifluoride (1.353 g, 6 mmol) were first dissolved in 10 ml *N*,*N*-dimethylacetamide (DMAc) in a 50 ml flask with stirring. After the mixture was completely dissolved, potassium carbonate (1.38 g, 10 mmol) was added to the solution in one portion. The mixture was stirred at room temperature for 30 min and then heated at 125 °C for 15 h. The obtained mixture was poured into acetic acid/water (volume ratio 1/9) to give a white solid, which was collected, washed thoroughly with water, and dried under vacuum at 80 °C. Yield: 92.3%. $C_{41}H_{24}F_9N_3O_9$ (873.14): Calcd C 56.37, H 2.77, N 4.81; Found C 56.12, H 2.91, N 4.86. ^{1}H NMR (DMSO-d_6): $\delta = 7.02-7.48$

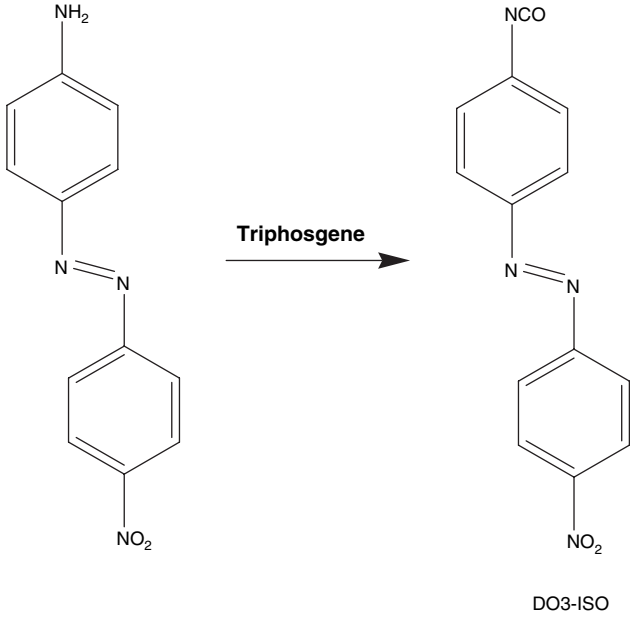

Scheme 2. Synthesis of 4-((4′-nitrophenyl)azo)phenylisocyanate dye.

and 8.23–8.54 (m, Ar-H), 2.23 (s, $-CH_3$). IR (KBr): 1046 and 1337 cm^{-1} (−CO), 3383, 1340 and 1525 cm^{-1} (NO_2).

2.5. Synthesis of 1,1,1-tris[4-(4-amino-2-trifluoromethylphenoxy)phenyl]ethane (compound **2**) (Scheme 3)

A suspension solution was prepared by mixing compound **1** (1.752 g, 2 mmol) with 10% Pd/C (0.45 g) in ethanol (75 ml). Hydrazine monohydrate (5 ml) was added to the stirred solution. The solution was then heated at reflux temperature for 4 h. The hot reaction solution was filtered to remove Pd/C and the filtrate was then distilled to remove the solvent. The obtained mixture was poured into water to wash away redundant hydrazine monohydrate. The precipitate was yellowish white crystals and further dried in vacuum at room temperature. Yield: 84.7%. $C_{41}H_{30}F_9N_3O_3$ (783.21): Calcd C 62.84, H 3.86, N 5.36; Found C 62.52, H 4.10, N 5.43. ^1H NMR (DMSO-d_6): $\delta = 6.41–7.15$ (m, Ar-H), 5.44 (s, $-NH_2$) and 2.03 (s, $-CH_3$). IR (KBr): 1046 and 1337 cm^{-1} (−CO), 3383 and 3467 cm^{-1} (NH_2).

2.6. MMT intercalated with 1,1,1-tris[4-(4-amino-2-trifluoromethylphenoxy)phenyl]ethane

An example of a preparative procedure for preparing wide *d*-spacing silicates is shown as follows. Na^+-MMT (1 g, 1.20 mequiv/g) was placed in a 250 ml flask and dispersed vigorously into 100 ml of deionized water at room temperature. In a separate vessel the precursor intercalating agent (compound **2**; 0.94 g, 1.20 mmol) was acidified with hydrochloric acid (37% in water, 0.18 g, 1.20 mmol, acidification ratio of $H^+/NH_2 = 1/3$) in 75 ml of ethanol. The solution was poured into the flask containing the swelled Na^+-MMT slurry. The

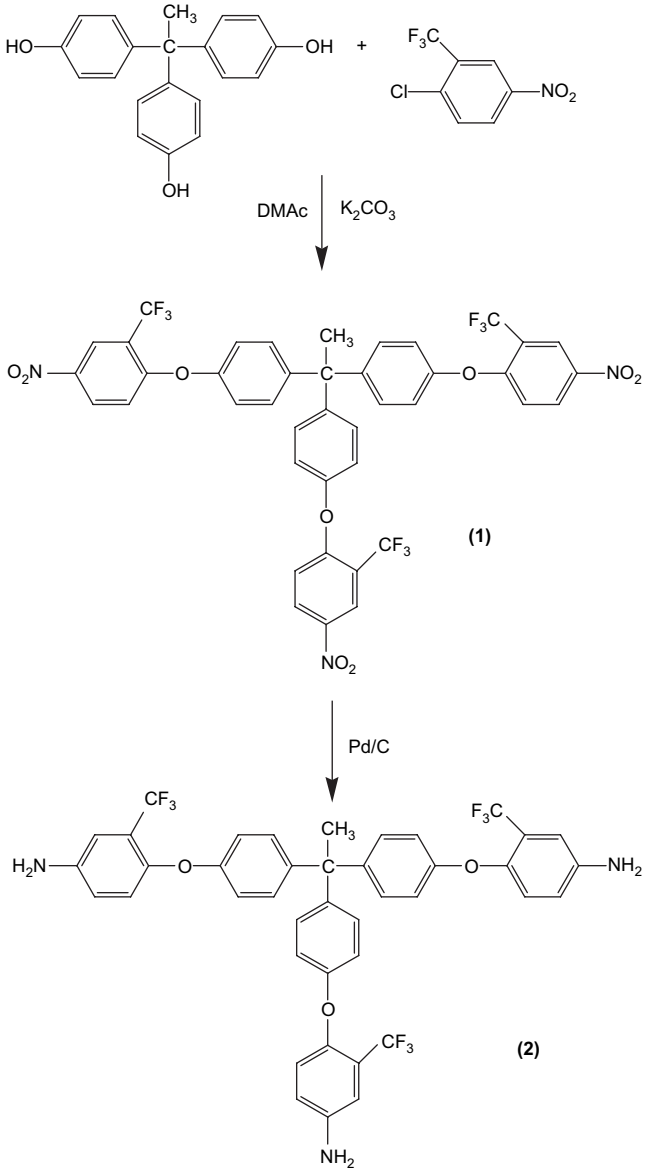

Scheme 3. Synthesis of intercalating agent.

mixture was stirred vigorously at 60 °C for 11 h and then allowed to cool to room temperature. The resulting agglomerated precipitate was collected and washed thoroughly with deionized water to remove the free amine. MMT/triamine was dried in a vacuum oven at 70 °C.

2.7. Synthesis of NLO side-chain polymer (PIDO3)

The following polymerization procedure exemplifies the synthesis of PIDO3 (Scheme 4). Polyimide (0.64 g, 1 mmol) was dissolved in 10 ml of dried THF in a 50 ml flask. DO3-ISO (0.536 g, 2 mmol) was dissolved in 20 ml of dried THF and then the solution was added to the polyimide solution dropwise. The mixture was heated at 70 °C for 48 h and then dried in a vacuum oven at 70 °C. The obtained mixture was extracted by chloroform for 24 h using a Soxhlet extractor and dried under vacuum at 70 °C. Yield: 81.2%. ^1H NMR

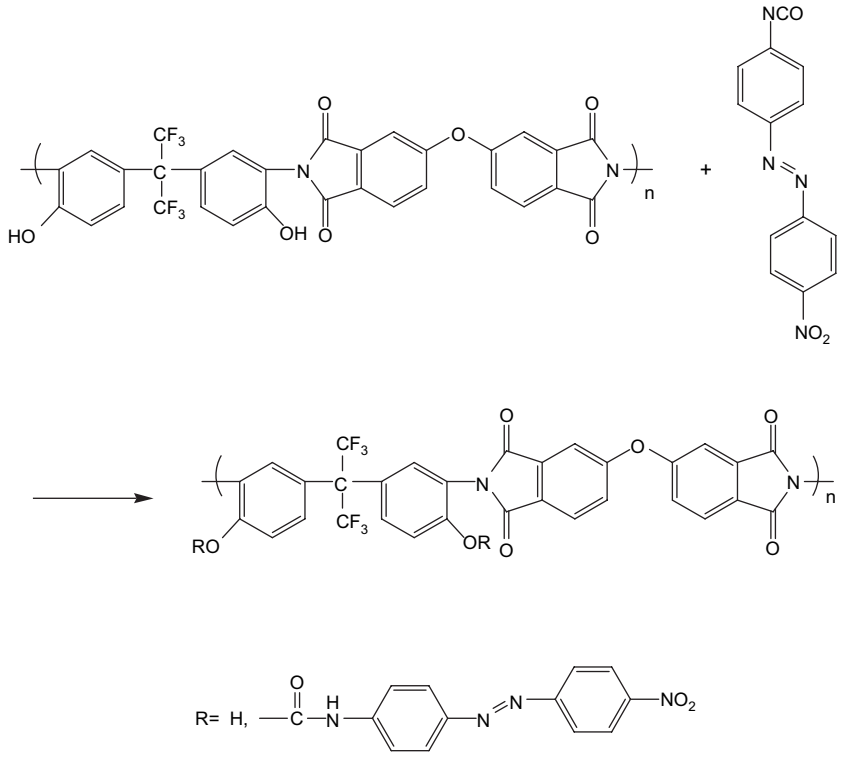

Scheme 4. Synthesis of NLO side-chain polymer (PIDO3).

(DMSO-d_6): $\delta = 6.6-6.8$, 7.7–8.1 and 8.3–8.4 (m, Ar-H of dye), 7.0–7.6 and 8.0–8.5 (m, Ar-H of polyimide). IR (KBr): 1380 cm^{-1} (C–N), 1720 and 1780 cm^{-1} (C=O), 1520 and 1342 cm^{-1} (NO_2).

2.8. Synthesis of polyimide/MMT nanocomposite (PDT system) (Scheme 1)

Poly(amic acid) (PAA) was synthesized by placing 2,2-bis(3-amino-4-hydroxypheny1)-hexafluoropropane (0.36626 g, 1 mmol) in 5 ml of dried DMAc in a 50 ml flask. After the diamine was dissolved completely, 4,4′-oxydiphthalic anhydride (0.3257 g, 1.05 mmol) was added to the diamine solution in one portion. Subsequently the mixture was stirred in an ice bath for 12 h. Polyimides consisting of swelling-agent-modified MMT were prepared in the following manner. A suspension solution was obtained by stirring the swelling-agent-modified MMT in DMAc for 12 h. The suspension was then added to PAA in DMAc to form PAA/organoclay samples with different weight ratios (1–10 wt%) of organoclay. The samples were subsequently heated at 160 °C for 2 h to form polyimide/organoclay samples. Afterward, an equal equivalent of NLO dye, DO3-ISO was reacted with respective polyimide/organoclay materials to acquire a series of NLO organic/inorganic hybrid polymers. They are PDT1C, PDT3C, PDT5C, PDT8C, and PDT10C as shown in Table 1.

2.9. Thin film preparation

These polyimide/organoclay materials were, respectively, dissolved in DMAc. The polymer solution was stirred at room temperature for 3 h and filtered through a 1 μm syringe filter. Thin films were prepared by spin coating the filtered polymer solution onto indium tin oxide (ITO) glass substrates. Prior to the poling process, these thin films were dried in vacuum at 60 °C for 24 h.

2.10. Poling process and electro-optical (EO) coefficient (r_{33}) measurement

The poling process for the second-order NLO polymer films was carried out using an in situ contact poling technique. The poling voltage was maintained at 100 V and the temperature was kept at approximately 10 °C lower than the T_g of the sample for a certain period of time. Upon saturation of the r_{33} signal intensity, the sample was then cooled down to room temperature in the presence of the poling field at which point the poling field was terminated. The thicknesses and indices of

Table 1
Thermal decomposition temperatures and glass transition temperatures of polyimide, PIDO3 and PDT samples

Sample	Content of organoclay (wt%)	T_d[a] (°C)	T_g (°C)
Polyimide	0	373.6	251.8
PIDO3	0	240.9	165.3
PDT1C	1	304.3	229.4
PDT3C	3	305.7	230.1
PDT5C	5	295.4	196.6
PDT8C	8	302.0	—[b]
PDT10C	10	290.9	—[b]

[a] T_d was determined at the temperature corresponding to 5 wt% weight loss.
[b] T_g was not detectable.

refraction were measured by a Spectroscopic Ellipsometer (J.A. Wollam Co., Inc., MW2000 at 830 nm). EO coefficients of the polarized samples were measured at 830 nm wavelength using the simple reflection technique [31].

2.11. Optical loss measurement

The laser beam (830 nm) passes through a linear polarizer and a polarizing beam splitter [32–34]. Then the TE polarized light is focused onto a prism coupler that is mounted on a rotation stage. The scattered light was imaged with an infrared-sensitive charge-injection device camera system. A statistical linear fit of the data to the logarithm of the scattered light intensity versus the distance propagated down the waveguide yielded a waveguide loss as a slope.

3. Results and discussion

3.1. Synthesis and characterization of side-chain NLO polyimides

The polyimide was synthesized using a traditional two-step synthetic method. This included a polycondensation between a diamine and dianhydride to form poly(amic acid) and a thermal imidization in DMAc to form a polyimide. Subsequently, the hydroxy-containing polyimide was reacted with the isocyanate-containing NLO dye, DO3-ISO. The structures of the polymers were confirmed by spectroscopic techniques such as FTIR and ^{1}H NMR. FTIR spectra of the hydroxyl-containing polyimide and PIDO3 samples are shown in Fig. 1. The spectra exhibited two characteristic absorption bands at 1720 and 1780 cm^{-1} due to the C=O stretching in imide ring, and a characteristic absorption band at 1380 cm^{-1} due to the C–N stretching in imide ring (Fig. 1(a)). These results support the formation of the imide groups. In addition, a very strong peak at 2260 cm^{-1} is associated with the isocyanate group of NLO dye, DO3-ISO (Fig. 1(b)). When the reaction between isocyanate and hydroxyl groups was completed, the peak of 2260 cm^{-1} (absorption of isocyanate) disappeared completely. As shown in Fig. 1(c), the characteristic absorption bands of the symmetrical and asymmetrical stretching of the nitro groups were also evident at approximately 1520 and 1342 cm^{-1}, respectively, clearly indicating the presence of the NLO dye in the polymer. ^{1}H NMR spectrum (DMSO-d_6) of PIDO3 exhibited chemical shifts around 6.6–6.8, 7.7–8.1, and 8.3–8.4 ppm corresponding to Ar-H of dye, and 7.0–7.6 and 8.0–8.5 ppm corresponding to Ar-H of polyimide [11]. The ratios of integrated areas conformed to the number of hydrogens, further confirming the successful incorporation of DO3-ISO onto the polyimide.

3.2. Morphology of organoclay

X-ray diffraction data of the pristine MMT, swelling-agent-modified MMT, and PDT samples are presented in Fig. 2. For the pristine MMT, a strong X-ray diffraction peak at $2\theta = 7.4°$ was caused by the diffraction of the (001) crystal surface of

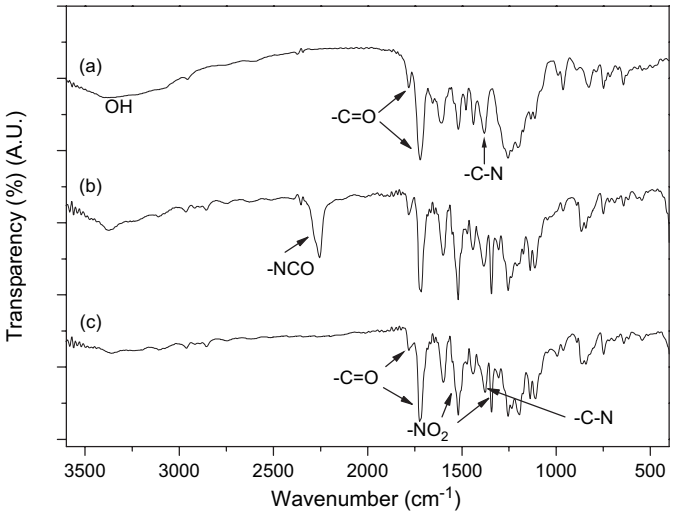

Fig. 1. Infrared spectra of (a) polyimide, (b) polyimide reacted with DO3-ISO for 0.5 h and (c) PIDO3.

layered silicates, equaling a d-spacing of 12 Å. In this spectrum, the d-spacing of swelling-agent-modified MMT based on Bragg's Law ($n\lambda = 2d \sin\theta$ and the observed values for $n = 1$, 2) was 27 Å. Additionally, the WAXD curves of PDT1C and PDT3C containing 1 and 3 wt% of swelling-agent-modified MMT, respectively, did not display any X-ray diffraction peak at $2\theta = 1.5–8.0°$, indicating that the d-spacing of silicate layers had been either intercalated to a distance of more than 59 Å or the silicate layers were exfoliated. While the organoclay content increased to the range from 5 to 10 wt%, the PDT samples showed a small diffraction peak at $2\theta = 6.9°$ ($d = 13$ Å) as opposed to the diffraction peak at $2\theta = 3.2°$ ($d = 27$ Å) for the swelling-agent-modified MMT. This implies that small amount of organoclay was not exfoliated in the polyimide [15]. The peak value indicates the possible presence of polyimide molecules outside the MMT

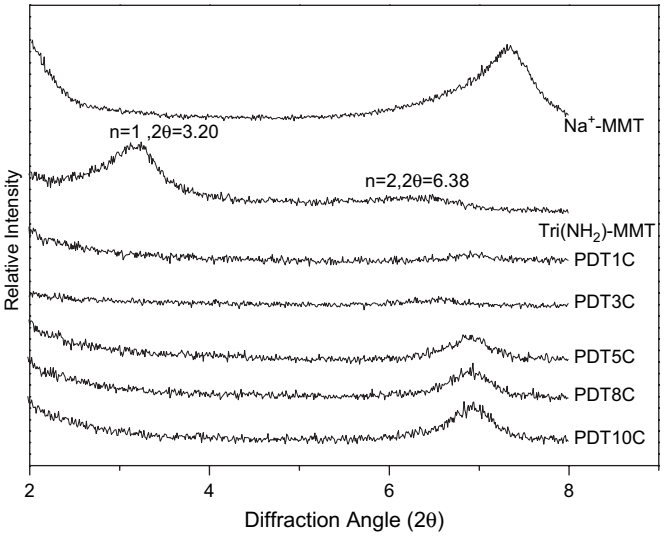

Fig. 2. X-ray diffraction patterns of MMT, swelling-agent-modified MMT and PDT series.

layers squeezed the clay layers during the solvent removal process, causing a reduction in the spacing between the layers [25,35].

The further evidence of this nanometer-scale dispersion of intercalated silicate layers in polyimide was investigated by TEM. Fig. 3 shows the TEM micrographs visualizing the spatial distribution among the PDT hybrids. As shown in Fig. 3(a), the TEM image of PDT8C exhibited a mixed morphology. Among individual silicate layers, only part of them were intercalated in the polyimide matrices, whereas the remnant displayed aggregated phenomenon. Intercalated silicate domains exhibiting a collection of 5–10 nearly parallel silicate layers with basal spacings of approximately 6–10 nm were observed. This *d*-spacing of layered silicates is larger than that (1.2 nm) of the pristine organoclay. Evidently, these silicate layers have been intercalated in the NLO-active polyimide. Apart from that, the aggregated phenomenon is possibly due to the number of polyimide polymer chains that is not large enough to resist the attraction between silicate interlayers [36]. Furthermore, the polyimide chains perhaps possessed the lying down conformation as they were slightly inserted into space between interlayer silicates [36]. When the content of clay decreased (PDT3C), plenty of polyimide chains would develop into an extended morphology and eventually form an exfoliated conformation. In Fig. 3(b), the TEM image of PDT3C indicates that silicate layers were uniformly dispersed in the polymer matrices, exhibiting primary exfoliated morphology. This is consistent with the study of powder X-ray diffraction patterns on the prepared sample in previous section. Similar exfoliated morphology was also observed for the PDT1C sample.

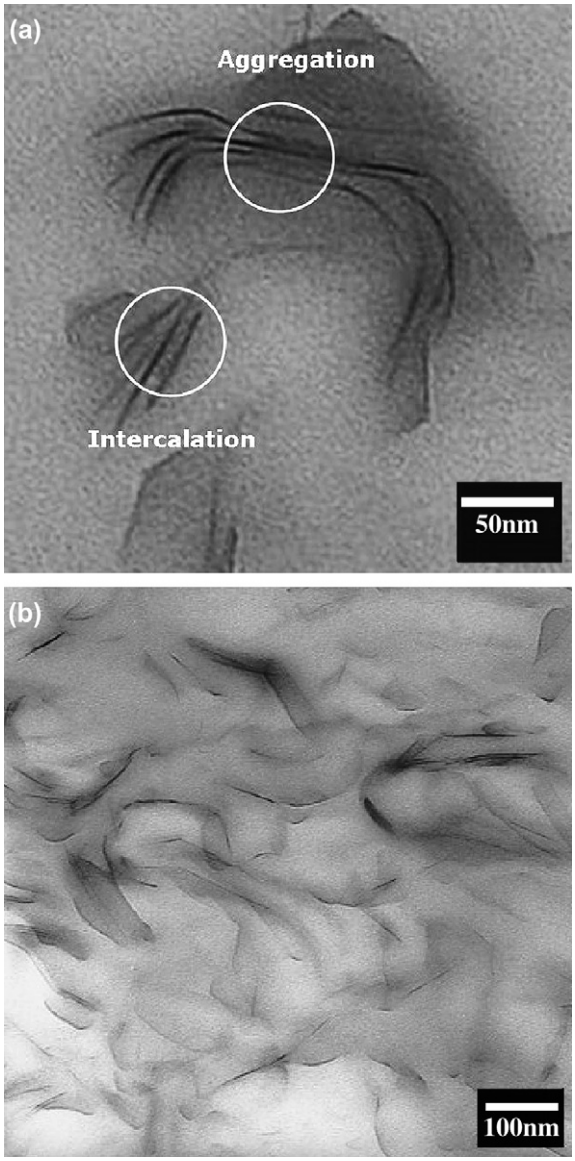

Fig. 3. Transmission electron micrographs of (a) PDT8C and (b) PDT3C.

3.3. Thermal stability

Thermal properties of the polyimide, PIDO3 and PDT samples are shown in Table 1. T_gs were measured using DSC and the T_g of the polyimide was observed at 251.8 °C. T_ds were measured using TGA under N_2 atmosphere, with regard to the weight loss of 5 wt%. The T_d of the polyimide was observed at 373.6 °C. In addition, the T_g of the polyimide functionalized with DO3 (PIDO3) was observed at 165.3 °C, whereas the T_d was observed at 240.9 °C. As the dyes were covalently attached to the side chain of polyimide, the T_g of the polymer decreased significantly. This might be due to the fact that the side-chain dyes prevented tight packing between polymer chains, leading to a decrease in intermolecular interactions [37]. Fig. 4 shows the TGA thermograms of PIDO3 and PDT1C. Two weight loss stages can be observed in the TGA thermograms. The first stage, at 300–350 °C, resulted from the decomposition of the side-chain NLO dyes, whereas the second stage, at a higher temperature range, resulted from the decomposition of the imide linkages [38]. Furthermore, the T_ds of these PDT samples were found to shift toward higher temperature ranges than that of the pristine polyimide sample,

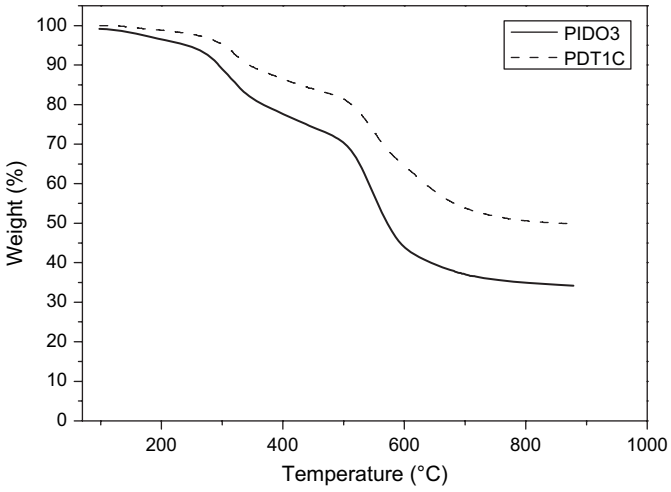

Fig. 4. TGA thermograms of PIDO3 and PDT1C.

PIDO3. This might result from the barrier effect of the MMT layer structures, as well as the strong interaction between the organoclay and polyimide [39–41]. In addition, the PDT1C and PDT3C samples exhibited increased T_gs as compared to the PIDO3 sample. This is due to the restriction of the intercalated polymer chains within the clay galleries. In other words, the molecular motions of the polyimide were inhibited by the silicate layers. However, further increase of clay loading (e.g. 5 wt%) was found to be incapable of enhancing the T_g of the PDT sample. This is possibly due to the aggregation of MMT as reported by other researchers [42]. The aggregation of the silicate layers indeed was observed in the TEM image (Fig. 3(a)) as mentioned in the previous section. In this system, only part of the silicate layers were intercalated in the polyimide matrices. As a result, the molecular motions of the polyimide chains were not restrained by the silicate layers effectively.

3.4. Optical properties

To generate stable oriented dipoles and large EO coefficients, NLO-active polymers should be aligned and annealed under an electronic field. Optical quality films were obtained by spin coating the PIDO3 and PDT solutions onto ITO glasses. Optical properties of these NLO materials are shown in Table 2. Refraction indices range from 1.65 to 1.68. It is important to note that the dye contents were determined by UV–vis spectroscopic investigations [43,44]. EO coefficients resulted from the in situ poling process are in the range between 4.6 and 8.0 pm/V (measured at 830 nm). It is important to note that these NLO-active polyimide/MMT materials are the first polyimide/MMT system capable of exhibiting NLO properties. This is possibly due to the fact that *d*-spacings of silicate layers were intercalated to a sufficient distance, or the silicate layers were exfoliated. Therefore, the dye-containing polyimide chains were not restricted between the silicate layers. In addition, recent theoretical analyses suggest that large *d*-spacings should be present to allow J-alignment formation, i.e. acentric arrangement of dyes [45]. As a result of this, the NLO properties would be obtained. Moreover, EO coefficients were depending upon the dye contents, which implies that the aggregation of NLO dyes did not take place in the above measured [8].

In the investigation of the transmission losses of the optical waveguides, only TE guide modes at 830 nm were considered.

Table 2
Optical properties of the polyimide and PDT samples

Sample	Contents of organoclay (wt%)	Dye content (wt%)	Refraction indices	Optical loss at 830 nm (dB/cm)	r_{33} (pm/V)
PIDO3	0	27.1	1.68	3.1	8.0
PDT1C	1	24.0	1.66	5.3	7.6
PDT3C	3	22.0	1.67	7.8	6.1
PDT5C	5	20.8	1.67	9.3	5.7
PDT8C	8	16.0	1.65	10.6	5.2
PDT10C	10	14.8	1.66	–	4.6

Optical loss was not detectable.

As shown in Table 2, the optical losses of the PIDO3 and PDT samples are in the range 3.1–10.6 dB/cm. Conspicuously, the optical loss was increased with increasing content of organoclay. Indeed, the organoclay could effectively improve thermal stability of materials, but the waveguide properties of the polymers were sacrificed simultaneously. Hence, further optimization of materials and processing conditions is needed to decrease the optical losses of the polymers. In fact, high optical loss can refer to the second harmonic (overtone) vibrational absorption of C–H bond in the near-infrared region, scattering loss from structure defect (void), and absorption loss from a charge-transfer interaction. These defects can be limited by shifting the high-absorption signal to longer wavelengths by replacing the hydrogen atoms with heavier atoms such as deuterium, chlorine or fluorine [46–48]. In this particular area, direct introduction of fluorine atoms to chromophores and polyimide structures seems to be able to readily provide lower optical losses [47].

In general, the NLO properties of polymers remain stable at low temperatures, but decays significantly at a specific temperature. This specific temperature is defined as the effective relaxation temperature [49]. The thermal dynamic behavior provides information on the maximum device operating temperatures that the film can suffer, and allows quick evaluation of the temporal and thermal stability of the materials [6]. In the investigation of dynamic thermal stability, only PIDO3 and the samples with better thermal stability (PDT1C) were measured at 830 nm. Fig. 5 shows dynamic thermal stability of the poled PIDO3 and PDT1C samples. At the temperature above room temperature, the r_{33} activity commenced to decrease with the increasing temperature. This might be due to the fact that some relaxation of local stresses accumulated by sample preparation would cause the randomization of aligned NLO dyes, leading to depression of NLO activity. Cheng et al. have reported the primary and secondary dielectric relaxation phenomena in an NLO polymer [50]. It was found that dielectric measurements on a typical NLO side-chain polymer exhibited multiple relaxation processes even

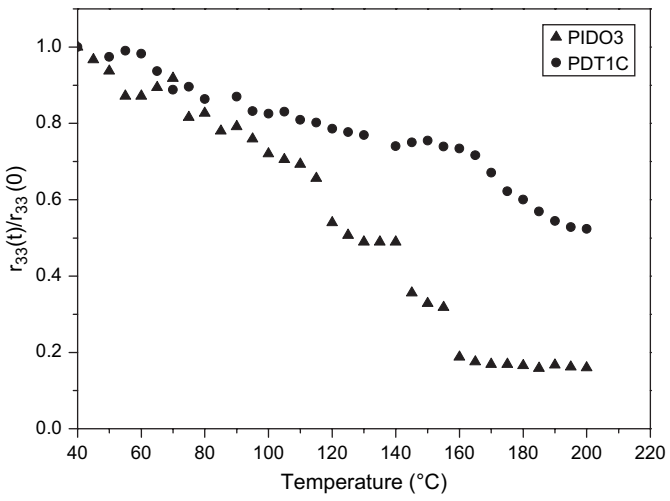

Fig. 5. Temperature dependence of the dipole re-orientational dynamics of the poled PIDO3 and PDT1C samples.

below room temperature, which are all related to the chemically attached chromophore dipoles. The results clearly show that chromophore dipoles are significantly mobile even below the T_g of the NLO polymer. Therefore, the r_{33} activity would begin to decrease at the temperature above room temperature. Similar phenomenon was also reported by other researchers [8,51,52]. Besides, PDT1C exhibits a higher effective relaxation temperature as compared to the pristine polyimide, PIDO3, indicating that the mobility of the aligned NLO dyes in PDT1C is more restricted than that in the pristine polyimide. This is due to the presence of strong interaction between the organoclay and polyimide molecules, as well as the barrier effect resulting from MMT layer structure. The result of dynamic thermal stability was consistent with the thermal properties' study mentioned earlier.

To investigate the long-term NLO stability of the poled polymers, dipole reorientation of the poled polymeric film was observed by measuring the EO coefficient ($r_{33}(t)/r_{33}(t_0)$) as a function of time at 100 °C. Fig. 6 shows the temporal stability of EO coefficient for the poled PIDO3 and PDT samples at 100 °C. At the beginning of thermal treatment, a fast decay of the EO coefficients was perceived. This phenomenon may result from recovery of bond angle and bond length of the oriented dyes [53–55]. Better temporal stability was obtained for the samples with the exfoliated MMT. This indicates that the incorporation of MMT can effectively enhance the stability of NLO properties. After being subjected to thermal treatment at 100 °C for 320 h, a reduction of less than 50% in the EO coefficient ($r_{33}(t)/r_{33}(t_0)$) was observed for all of the poled PDT samples. It is important to note that the PDT5C and PDT10C samples exhibited poorer temporal stability than the PDT1C and PDT3C samples. This is due to the aggregation of MMT layer structures in the PDT5C and PDT10C samples, as shown in the TEM mapping study previously. Moreover, in comparison with the poled PIDO3 sample, the poled PDT1C and PDT3C samples exhibited much better temporal stability. This is a direct consequence of the polymer chains within the clay galleries capable of suppressing the mobility of the aligned NLO dyes.

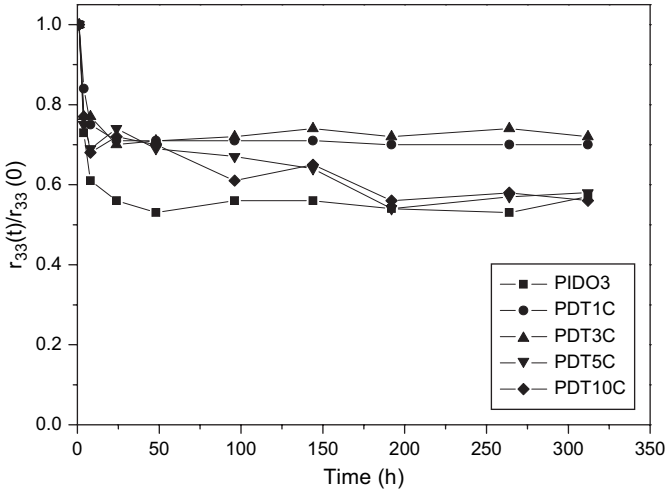

Fig. 6. Temporal behavior of the EO coefficient for the poled PIDO3 and PDT samples at 100 °C.

4. Conclusion

A specially designed reactive swelling agent containing multiple functional groups was used. Exfoliation of layered silicates in the polyimide matrices has been achieved. Furthermore, this ameliorated morphology of polyimide/organoclay materials due to the presence of chemical bonding between the swelling-agent-modified MMT and polymer molecules would result in enhanced thermal properties. These polyimide/organoclay materials have been shown to possess excellent dimensional stability and excellent optical transparency. EO coefficients of these polyimide/inorganic materials are in the range of 4.6 and 8.0 pm/V. To our knowledge, these NLO-active polyimide/MMT materials are the first polyimide/MMT system capable of exhibiting NLO properties. The polyimide/MMT systems exhibited much better long-term NLO stability than the pristine polyimide system.

Acknowledgements

Financial support from National Science Council of Taiwan and Chung Shan Institute of Science and Technology is gratefully acknowledged. The authors also thank Education Ministry of Taiwan for funding Center for Advanced Industry Technology and Precision Processing, NCHU.

References

[1] Qin A, Yang Z, Bai F, Ye C. Design and synthesis of a thermally stable second-order nonlinear optical chromophore and its poled polymers. J Polym Sci Part A Polym Chem 2003;41:2846–53.
[2] Luo J, Cheng YJ, Kim TD, Hau S, Jang SH, Shi Z, et al. Facile synthesis of highly efficient phenyltetraene-based nonlinear optical chromophores for electrooptics. Opt Lett 2006;8:1387–90.
[3] Kim TD, Luo J, Tian Y, Ka JW, Tucker NM, Haller M, et al. Diels–Alder "Click Chemistry" for highly efficient electrooptic polymers. Macromolecules 2006;39:1676–80.
[4] Sullivan PA, Akelaitis AJP, Lee SK, McGrew G, Lee SK, Choi DH, et al. Novel dendritic chromophores for electro-optics: influence of binding mode and attachment flexibility on electro-optic behavior. Chem Mater 2006;18:344–51.
[5] Kuo WJ, Chang MC, Juang TY, Chen CP, Chen CT, Chang HL, et al. Stable second-order NLO semi-IPN system based on bipyridine-containing polyimide and alkoxysilane dye. Polym Adv Technol 2005;16:515–23.
[6] Hsiue GH, Kuo WJ, Lin CH, Jeng RJ. Preparation and characterization of all organic NLO sol–gel materials based on amino azobenzene dyes. Macromol Chem Phys 2000;201(17):2336–47.
[7] Jeng RJ, Chen YM, Chen JI, Kumar J, Tripathy SK. Phenoxysilicon polymer with stable second-order optical nonlinearity. Macromolecules 1993;26:2530–4.
[8] Chen CP, Huang GS, Jeng RJ, Chou CC, Su WC, Chang HL. Low loss second-order non-linear optical crosslinked polymers based on a phosphorus-containing maleimide. Polym Adv Technol 2004;15:587–92.
[9] Jeng RJ, Chang CC, Chen CP, Chen CT, Su WC. Thermally stable crosslinked NLO materials based on maleimides. Polymer 2003;44:143–55.
[10] Jeng RJ, Hung WY, Chen CP, Hsiue GH. Organic/inorganic NLO materials based on reactive polyimides and a bulky alkoxysilane dye via sol/gel process. Polym Adv Technol 2003;14:66–75.

[11] Lu J, Yin J. Synthesis and characterization of photocrosslinkable, side-chain, second-order nonlinear optical poly(ester imide)s with great film-forming ability and long-term dipole orientation stability. J Polym Sci Part A Polym Chem 2003;41(2):303–12.
[12] Hsiue GH, Kuo JK, Jeng RJ, Chen JI, Jiang XL, Marturunkakul S, et al. Stable second-order nonlinear optical polymer network based on an organosoluble polyimide. Chem Mater 1994;6(7):884–7.
[13] Jeng RJ, Chen YM, Jain AK, Kumar J, Tripathy SK. Stable second-order nonlinear optical polyimide/inorganic composite. Chem Mater 1992;4(6):1141–4.
[14] Wang WJ, Chin WK, Wang WJ. Synthesis and structural characterizations of [chromophore]$^+$-saponite/polyurethane nanocomposites. J Polym Sci Part B Polym Phys 2002;40(15):1690–703.
[15] Tyan HL, Liu YC, Wei KH. Thermally and mechanically enhanced clay/polyimide nanocomposite via reactive organoclay. Chem Mater 1999;11:1942–7.
[16] Huang YP, Chen HY, Lee W, Tsai TY, Chin WK. Transient behaviour of polarity-reversed current in a liquid-crystal–montmorillonite–clay device. Nanotechnology 2005;16:590–4.
[17] Tsai TY, Huang YP, Chen HY, Lee W, Chang YM, Chin WK. Electro-optical properties of a twisted nematic–montmorillonite–clay nanocomposite. Nanotechnology 2005;16:1053–7.
[18] Ogawa M, Takizawa Y. Intercalation of alkylammonium cations into a layered titanate in the presence of macrocyclic compounds. Chem Mater 1999;11(1):30–2.
[19] Tyan HL, Leu CM, Wei KH. Effect of reactivity of organics-modified montmorillonite on the thermal and mechanical properties of montmorillonite/polyimide nanocomposites. Chem Mater 2001;13:222–6.
[20] Usuki A, Kawasumi M, Kojima Y, Okada A, Kurauchi T, Kamigaito O. Swelling behavior of montmorillonite cation exchanged for ω-amino acids by ε-caprolactam. J Mater Res 1993;8:1174–8.
[21] Usuki A, Kojima Y, Kawasumi M, Okada A, Fukushima Y, Kurauchi T, et al. Synthesis of nylon 6–clay hybrid. J Mater Res 1993;8:1179–84.
[22] Agag T, Koga T. Studies on thermal and mechanical properties of polyimide–clay nanocomposites. Polymer 2001;42:3399–408.
[23] Yu YH, Yeh JM, Liou SJ, Chen CL, Liaw DJ, Lu HY. Preparation and properties of polyimide-clay nanocomposite materials for anticorrosion application. J Appl Polym Sci 2004;92:3573–82.
[24] Morgan AB, Gilman JW, Jackson CL. Characterization of the dispersion of clay in a polyetherimide nanocomposite. Macromolecules 2001;34(8):2735–8.
[25] Yano K, Usuki A, Okada A. Synthesis and properties of polyimide–clay hybrid films. J Polym Sci Part A Polym Chem 1997;35(11):2289–94.
[26] Lan T, Kaviratna PD, Pinnavaia TJ. On the nature of polyimide–clay hybrid composites. Chem Mater 1994;6(5):573–5.
[27] Yang C, Zhou H, Chen X, Liu Y, Qin J. Synthesis and characterization of intercalation compounds of stilbazolium chromophores into layered vanadyl phosphate. J Mater Chem 2005;15:1637–9.
[28] Wang X, Balasubramanian S, Kumar J, Tripathy SK. Azo chromophore-functionalized polyelectrolytes. 1. Synthesis, characterization, and photoprocessing. Chem Mater 1998;10(6):1546–53.
[29] Chen TA, Jen AK-Y, Cai Y. A novel class of nonlinear optical side-chain polymer: polyquinolines with large second-order nonlinearity and thermal stability. Chem Mater 1996;8(3):607–9.
[30] Lee SH, Balasubramanian S, Kim DY, Viswanathan NK, Bian S, Kumar J, et al. Azo polymer multilayer films by electrostatic self-assembly and layer-by-layer post azo functionalization. Macromolecules 2000;33(17):6534–40.
[31] Teng CC, Man HT. Simple reflection technique for measuring the electro-optic coefficient of poled polymers. Appl Phys Lett 1990;56(18):1734–7.
[32] Shi W, Fang CS, Pan QW, Gu QT, Xu D, Wei HZ, et al. Measurement of the optical transmission modes and losses of the poled guest–host polymer NAEC/PEK-c planar waveguides. Opt Lasers Eng 2000;33(1):21–8.
[33] Shi W, Fang CS, Sui Y, Yin J, Pan QW, Gu QT, et al. Poling optimization and optical loss measurement of the polyetherketone polymer films. Solid State Commun 2000;116:67–71.
[34] Shi W, Fang CS, Sui Y, Yin J, Pan QW, Gu QT, et al. Thermal stability and transmission losses of the poled polyimide side-chain thin films. Opt Commun 2000;183:299.
[35] Chang JH, Park DK, Ihn KJ. Polyimide nanocomposite with a hexadecylamine clay: synthesis and characterization. J Appl Polym Sci 2002;84(12):2294–301.
[36] Juang TY, Tsai CC, Wu TM, Dai SA, Chen CP, Lin JJ, et al. Organo-clay hybrids based on dendritic molecules: preparation and characterization. Nanotechnology 2007;18:205606.
[37] Sui Y, Liu YG, Yin J, Gao J, Zhu ZK, Huang DY, et al. Study on side-chain second-order nonlinear optical polyimides based on novel chromophore-containing diamines. I. Synthesis and characterization. J Polym Sci Part A Polym Chem 1999;37(23):4330–6.
[38] Sui Y, Lu JX, Yin J, Wang D, Zhu ZK, Wang ZG. High T_g second-order nonlinear optical poly(urethane-imide)s prepared from disperse Red 19, pyromellitic dianhydride, and tolylene diisocyanate. J Appl Polym Sci 2002;85(5):944–9.
[39] Yeh JM, Liou SJ, Lin CY, Cheng CY, Chang YW. Anticorrosively enhanced PMMA–clay nanocomposite materials with quaternary alkylphosphonium salt as an intercalating agent. Chem Mater 2002;14(1):154–61.
[40] Yeh JM, Chen CL, Kuo TH, Su WF, Huang HY, Liaw DJ, et al. Preparation and properties of (BATB–ODPA) polyimide–clay nanocomposite materials. J Appl Polym Sci 2004;92(2):1072–9.
[41] Petrovic XS, Javni I, Waddong A, Banhegyi GJ. Structure and properties of polyurethane–silica nanocomposites. J Appl Polym Sci 2000;76(2):133–51.
[42] Tyan HL, Wei KH, Hsieh TE. Mechanical properties of clay–polyimide (BTDA–ODA) nanocomposites via ODA-modified organoclay. J Polym Sci Part B Polym Phys 2000;38(22):2873–8.
[43] Song N, Men L, Gao JP, Bai Y, Beaudin AMR, Yu G, et al. Cross-linkable zwitterionic polyimides with high electrooptic coefficients at telecommunication wavelengths. Chem Mater 2004;16(19):3708–13.
[44] Luo JD, Haller M, Li HX, Tang HZ, Jen AK-Y. A side-chain dendronized nonlinear optical polyimide with large and thermally stable electrooptic activity. Macromolecules 2004;37(2):248–50.
[45] Coradin T, Veber M, Francis AH, Clement R. The $MnPS_3$ layered phase as a substrate for aggregate formation: the example of triarylpyrylium cations. J Mater Chem 1998;8(6):1471–5.
[46] Gao H, Wang D, Guan S, Jiang W, Jiang Z, Gao W, et al. Fluorinated hyperbranched polyimide for optical waveguides. Macromol Rapid Commun 2007;28:252–9.
[47] Campbell VE, Paoprasert P, Mykietyn JD, In I, Mcgee DJ, Gopalan P. Linear and branched fluoroazo-benzene chromophores with increased compatibility in semifluorinated polymers. J Polym Sci Part A Polym Chem 2007;45:3166–77.
[48] Kim E, Cho SY, Yeu DM, Shin SY. Low optical loss perfluorinated methacrylates for a single-mode polymer waveguide. Chem Mater 2005;17(5):962–6.
[49] Tsutsumi N, Moridhima M, Sakai W. Nonlinear optical (NLO) polymers. 3. NLO polyimide with dipole moments aligned transverse to the imide linkage. Macromolecules 1998;31(22):7764–9.
[50] Cheng ZY, Yilmaz S, Wirges W, Bauer-Gogonea S, Bauer S. Temperature-domain analysis of primary and secondary dielectric relaxation phenomena in a nonlinear optical side-chain polymer. J Appl Phys 1998;83(12):7799–807.
[51] Li Z, Qin J, Yang Z, Ye C. Synthesis and nonlinear optical properties of polyphosphazenes with binaphtholyl and indole side groups. J Appl Polym Sci 2007;104:365–71.
[52] Hayden LM, Brower SC, Strutz SJ. Pressure dependence of the depoling temperature in nonlinear optical polymers. Macromolecules 1997;30:2734–7.
[53] Clays K, Coe BJ. Design strategies versus limiting theory for engineering large second-order nonlinear optical polarizabilities in charged organic molecules. Chem Mater 2003;15(3):642–8.
[54] Tsai HC, Yu IC, Chang PH, Yu DC, Hsiue GH. Novel π-electron extension system via chromophores self-polymerization to enhance the NLO efficiency. Macromol Rapid Commun 2007;28:334–9.
[55] Centore R, Riccio P, Fusco S, Carella A, Quatela A, Schutzmann S, et al. Nonlinear optical properties of regioregular main-chain polyesters. J Polym Sci Part A Polym Chem 2007;45:2719–25.